Article

Cell Chemical Biology

HTiP: High-Throughput Immunomodulator Phenotypic Screening Platform to Reveal IAP Antagonists as Anti-cancer Immune Enhancers

Graphical Abstract

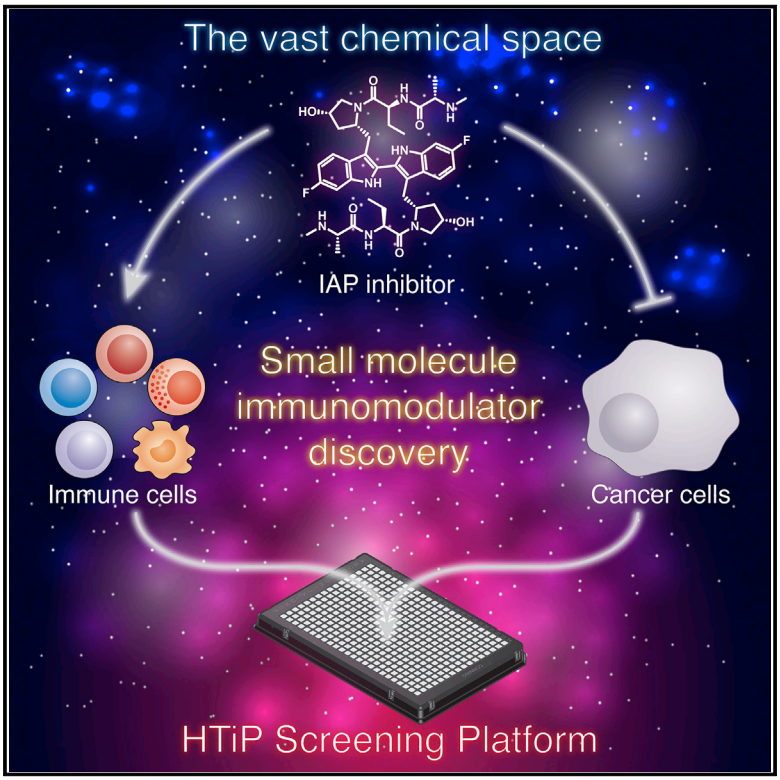

Authors

Xiulei Mo, Cong Tang, Qiankun Niu, Tingxuan Ma, Yuhong Du, Haian Fu

Correspondence

hfu@emory.edu

In Brief

Exploring the vast chemical space for immunotherapeutic agent discovery requires robust technologies that recapitulate the tumor-immune microenvironment. Mo et al. developed an HTiP platform that models the KRAS mutation-driven immunosuppressive phenotype. The identification of IAP inhibitors with known anti-tumor immunity activity supports the utility of HTiP to uncover small-molecule anti-cancer immunomodulators.

Highlights

- HTiP is a miniaturized co-culture system with cancer and immune cells
- HTiP integrates imaging- with biochemical-based readouts for built-in counterscreening
- HTiP models oncogenic KRAS mutation-induced immunosuppression
- HTiP screening identifies IAP inhibitors as anti-tumor immunity enhancers

Mo et al., 2019, Cell Chemical Biology *26*, 331–339
March 21, 2019
https://doi.org/10.1016/j.chembiol.2018.11.011

CellPress

Cell Chemical Biology
Article

HTiP: High-Throughput Immunomodulator Phenotypic Screening Platform to Reveal IAP Antagonists as Anti-cancer Immune Enhancers

Xiulei Mo,[1] Cong Tang,[1,2] Qiankun Niu,[1] Tingxuan Ma,[1] Yuhong Du,[1] and Haian Fu[1,3,4,*]
[1]Department of Pharmacology and Emory Chemical Biology Discovery Center, Emory University School of Medicine, Atlanta, GA 30322, USA
[2]Department of Urology, The First Affiliated Hospital, Medical School of Xi'an Jiaotong University, Xi'an, Shannxi 710061, People's Republic of China
[3]Department of Hematology and Medical Oncology and Winship Cancer Institute, Emory University, Atlanta, GA 30322, USA
[4]Lead Contact
*Correspondence: hfu@emory.edu
https://doi.org/10.1016/j.chembiol.2018.11.011

SUMMARY

Protein- and cell-based immunotherapeutic agents have revolutionized cancer treatment. However, small-molecule immunomodulators with favorable pharmacological properties for reaching intracellular targets remain to be developed. To explore the vast chemical space, a robust method that recapitulates the complex cancer-immune microenvironment in a high-throughput format is essential. To address this critical gap, we developed a high-throughput immunomodulator phenotypic screening platform, HTiP, which integrates the immune and cancer cell co-culture system with imaging- and biochemical-based multiplexed readouts. Using the HTiP platform, we have demonstrated its capability in modeling an oncogenic KRAS mutation-driven immunosuppressive phenotype. From a bioactive chemical library, multiple structurally distinct compounds were identified, all of which target the same class of proteins, inhibitor of apoptosis protein (IAP). IAP has demonstrated roles in cancer immunity. Identification of IAP antagonists as potent anti-tumor immune enhancers provides strong validating evidence for the use of the HTiP platform to discover small-molecule immunomodulators.

INTRODUCTION

Protein- and cell-based cancer immunotherapy has led to a paradigm shift in cancer treatment through modulating the immune system using immune checkpoint blocking antibodies and engineered chimeric antigen receptor T cells (Fesnak et al., 2016; Postow et al., 2015). Despite the clinical success of current immunotherapies for some cancers, the limitations of these therapies have come to light, such as the emerging clinical observation of limited response, the enormous economic burden of production and delivery, the complexity of pharmacokinetics, and the potential safety issue of immunogenicity (Chames et al., 2009; Fesnak et al., 2016; Sadelain et al., 2017).

To complement and potentially synergize with the immunotherapeutic antibodies and engineered immune cells, alternative therapeutic agents such as small-molecule immunomodulators remain to be developed (Dhanak et al., 2017). Small molecules offer a number of advantages, including improved bioavailability, enhanced tissue penetration, and the capability to reach intracellular targets of both immune and cancer cells. Moreover, small molecules could also serve as chemical probes for investigating mechanisms involved in anti-tumor immunity. Although there is an emerging effort in target-based screenings to identify small molecules that modulate a specific protein target (Dhanak et al., 2017; Huxley et al., 2004; Skalniak et al., 2017), phenotypic screenings reflecting the complex immune response network for large-scale high-throughput small-molecule immunomodulator discovery are highly challenging and remain to be established.

To address this critical gap in chemical immunomodulator discovery, we report a high-throughput immunomodulator phenotypic screening platform, HTiP, which integrates an immune and cancer cell co-culture system with imaging- and cell viability-based multiplexed readouts in a miniaturized format. As a proof of concept, we screened a focused chemical library of clinical and pre-clinical bioactive compounds and identified a group of inhibitor of apoptosis protein (IAP) antagonists as potent inducers of anti-tumor immunity that selectively suppress the growth of cancer cells with an oncogenic KRAS mutation.

RESULTS

Design and Development of the HTiP Screening Platform

To accelerate the discovery of small-molecule immunomodulators, a sensitive and scalable high-throughput technology platform that models the tumor microenvironment with human immune components in a high-density plate format is essential. Toward the goal of modeling the human cancer-immune interactions for high-throughput screening, we examined the feasibility of an *in vitro* co-culture system with both immune and cancer cells and tested it in a miniaturized 384-well plate format (Figure 1A). The co-culture system consists of label-free native human peripheral blood mononuclear cells (PBMCs) and cancer

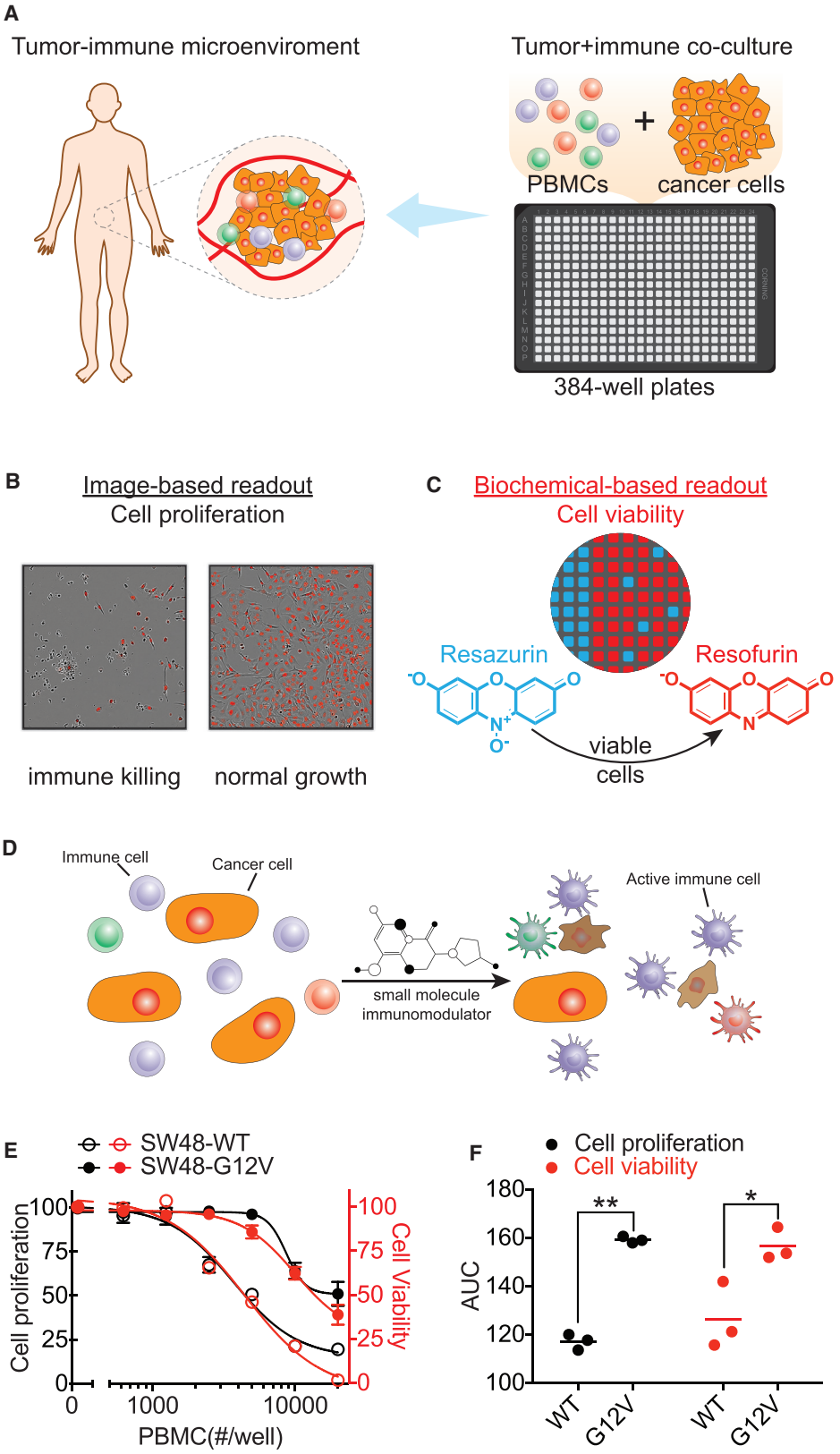

(legend on next page)

cells with oncogenic alterations. Human PBMCs containing a mixture of lymphocytes, monocytes, and dendritic cells were used to recapitulate the complexity of the immune system. The growth phenotype of cancer cells was monitored by an imaging system based on their differential sizes (Figure 1B). For the same well, cell viability was measured using a biochemical readout of the fluorescence intensity of resofurin produced in viable cells (Figure 1C). These dual readouts from the same well provide orthogonal cancer cell growth status that is designed to help triage potential false positives due to intrinsic artifacts of each method. For example, the artifacts from uneven cell distribution or clustering-induced biased image acquisition, and shade-off and halo-hindered automated phase-contrast image segmentation, and fluorescent compound interference may lead to false discovery for image-based high-content and fluorescence-based high-throughput screenings, respectively. The simplicity and dual readouts of the design enable the screening of large chemical libraries to identify compounds that stimulate or potentiate immune cells to attack cancer cells (Figure 1D).

The HTiP Platform Captures the Oncogenic KRAS-Induced Immune Suppression Phenotype

To examine whether the *in vitro* co-culture system can model the *in vivo* cancer immune surveillance mechanism, we first tested its capability to capture oncogene-induced immunosuppressive phenotypes. As a proof of principle, we selected cancer cell lines with an engineered KRAS G12V mutation to examine their growth phenotype under immune surveillance conditions using the *in vitro* co-culture system. Cancer cells carrying KRAS mutations have been reported to exert an immunosuppression phenotype via various molecular mechanisms (Chen et al., 2017; Kortlever et al., 2017; Zdanov et al., 2016).

Three pairs of isogenic cell lines, parental SW48, LIM1215, and NCI-H838 cells with KRAS wild-type (WT), and their corresponding genetically engineered KRAS G12V knockin cells with defined and matched genetic backgrounds, were subjected to the test. Native non-labeled human PBMCs were added to reconstitute the immune component, and the growth phenotypes of cancer cells were monitored. With the increasing number of immune cells, a dose-dependent PBMC-induced growth inhibition of KRAS WT cells was observed, whereas the effect was significantly attenuated in cells with KRAS G12V (Figures 1E and 1F), capturing the reported immunosuppressive phenotype of cancer cells with a KRAS mutation. In agreement with the image-based cell proliferation readout, the biochemical-based orthogonal cell viability measurement showed significantly more viable cells with G12V than with the WT KRAS with the same PBMC treatment (Figures 1E and 1F). These results altogether indicate that the oncogenic KRAS mutation-induced immune escape phenotype could be recapitulated using both readouts.

HTiP Screening Reveals Potential Anti-tumor Inducers

To examine the utility of the co-culture system to discover chemical immunomodulators, we collected and screened the Emory Enriched Bioactive Library (EEBL), a library of 2,036 bioactive compounds, including U.S. FDA-approved drugs with the potential for repurposing the existing drugs. For the primary screening, we utilized the SW48-G12V cell line and selected the 90% maximal effective concentration (EC_{90}) condition with a PBMC/cancer cell ratio of 5, which was based on our assessment of the assay window and robustness in both image-based cell growth measurement and biochemical-based cell viability readout (Figure S1).

Using this established condition for SW48-G12V, we performed primary parallel screenings in the presence or absence of PBMCs to assess the immune-mediated anti-cancer effects of small-molecule compounds. The parallel screenings exhibited robust performance, with signal-to-background (S/B) > 10 and Z' > 0.5 from both readouts (Figure S1). The immune killing selectivity index, which was defined as the ratio of percentage inhibition of cancer cell growth with immune cells to that without immune cells, was established for each compound to prioritize potential hits based on the potency of immune cell-dependent inhibition of cancer cell growth (Figure 2A). Based on the ranking of ''immune killing selectivity'' index of >1.5-fold and the inhibitory effect of <20% on SW48-G12V cancer cells in the absence of PBMCs from both readouts, the top ten hit compounds with double-positive readouts were prioritized for dose-response studies (Figure 2B).

Through the dose-response confirmatory assay with cherry-picked and newly purchased compounds, three of ten primary hits were validated with significant and reproducible effect in inducing immune cell-dependent inhibition of cell growth and viability (Figures 2C–2F). The other seven primary hits were triaged due to their low potency or lack of consistent effect (data not shown).

Multiple Small-Molecule Anti-cancer Immune Enhancers Target IAP Proteins

Among the positive-hit compounds, birinapant (Figure 2C), a second mitochondrial-derived activator of caspase (SMAC)-mimetic, small-molecule antagonist of IAP family proteins, showed a high immune killing selectivity index of >3 from the primary screening. In the dose-response study, birinapant exhibited a potent effect on immune cell-dependent inhibition

Figure 1. Development of Phenotypic Small-Molecule Immunomodulator Discovery Platform

(A) The 384-well plate-based immune and cancer cell co-culture system to model the human cancer-immune microenvironment.

(B) Image-based readout for monitoring cancer cell proliferation.

(C) Biochemical-based readout for measuring cell viability using fluorescent signal of resofurin from viable cells.

(D) Principle for screening of small molecules with capability to induce immune cell-mediated killing of cancer cells.

(E) PBMC-dose-dependent killing curves for KRAS WT and G12V isogenic SW48 cell lines. The data are presented as mean ± SEM from four independent experiments.

(F) Area under the curve (AUC) analysis of PBMC-dose-dependent killing curves of 3 pairs of KRAS WT and G12V isogenic cell lines. Each dot represents one cell line and the horizontal lines indicate the mean. *$p < 0.05$, **$p < 0.01$.

See also Figures S1 and S2.

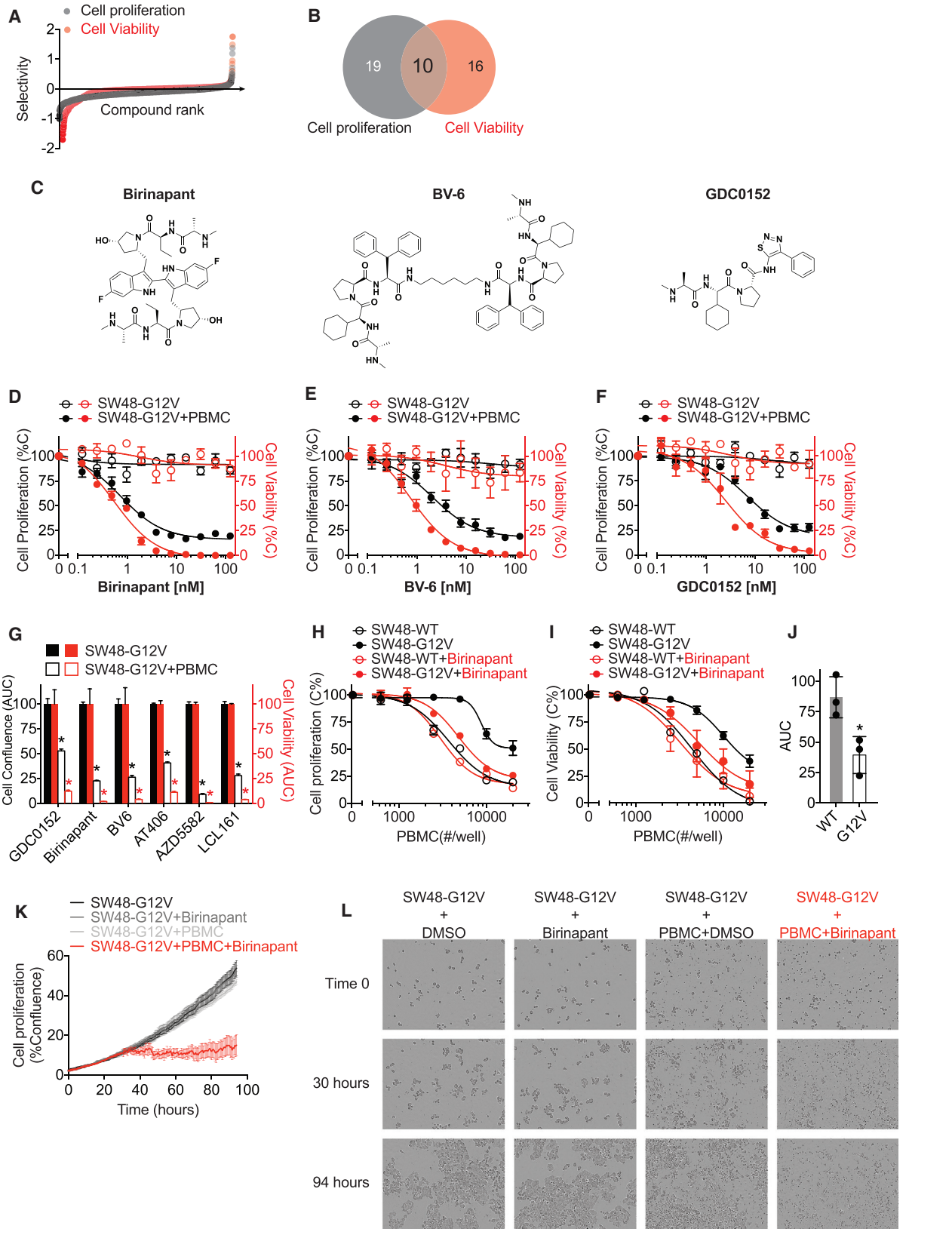

(legend on next page)

of cell growth and viability (Figure 2D) with desired selectivity. Birinapant showed little effect on the proliferation of SW48-G12V cells in the absence of PBMCs, while it exhibited a highly potent inhibitory effect on these cells in the presence of PBMCs, with a half-maximal inhibitory concentration (IC_{50}) of 0.7 ± 1.2 nM (Figure 2D). In agreement with the image-based readout, the biochemical-based cell viability readout recaptured the specific immune cell-dependent inhibition induced by birinapant, with an IC_{50} of 0.5 ± 0.2 nM. Interestingly, two structurally distinct positive hits identified from the screening, BV-6 and GDC0152, also belong to the class of IAP antagonists (Figure 2C). Both BV-6 and GDC0152 were confirmed in dose-response experiments, showing potent effects and selectivity in suppression of SW48-G12V cells, with an IC_{50} in the low nanomolar range (IC_{50} of 2.1 ± 1.3 and 7.0 ± 1.3 nM for BV-6 and GDC0152, respectively, in image-based assay; IC_{50} of 0.7 ± 1.1 and 2.5 ± 1.3 nM for BV-6 and GDC0152, respectively, in viability assay) (Figures 2E and 2F). These data support a general immune modulation function of these IAP antagonists, demonstrating the utility of our *in vitro* co-culture system in the high-throughput discovery of small-molecule immunomodulators.

To further support the specific impact of targeting IAP for immunomodulation, we purchased three additional IAP inhibitors, AT406, AZD5582, and LCL161, and tested their effects using the HTiP platform. In support of this notion, we found that these three IAP inhibitors induced immune cell-dependent selective killing of cancer cells with potencies in the nanomolar range (Figures 2D–2G and S2). In contrast, embelin, a promiscuous compound with IAP inhibitory effect in the micromolar range (Nikolovska-Coleska et al., 2004), failed to induce cancer cell death regardless of the presence of immune cells at 2 μM in the primary HTiP screening. Such convergent immunoregulatory effects from structurally divergent IAP inhibitors further reinforce the function of IAP in shaping anti-tumor immunity.

To evaluate the immune cell dependency of cancer cell selectivity for the identified IAP antagonists, we first used the isogenic WT and G12V SW48 cell lines to test their response to varying levels of immune cells upon compound treatment. Birinapant was used due to its potent immunomodulatory effect (Figure 2D). The PBMC dose-dependent cell growth inhibition curves were profiled in the presence of birinapant or with DMSO. As shown in Figures 1E and 1F, SW48-G12V showed reduced sensitivity to PBMC compared with SW48 WT. Birinapant treatment reversed such a resistance phenotype, showing significantly enhanced PBMC-dependent growth inhibition of KRAS G12V-mutation cells compared with the DMSO control (Figures 2H and 2I). In contrast, this compound failed to show enhanced immune cell killing of KRAS WT cells, exhibiting its cancer cell selectivity. In addition to the human engineered exogenous KRAS isogenic cell line model, patient-derived cancer cell lines with differential KRAS mutation status were tested for their sensitivity to birinapant in the HTiP assay (Figure S3). As shown in Figure 2J, human colorectal carcinoma cell lines carrying oncogenic KRAS mutations exhibited increased sensitivity to birinapant-triggered immune-dependent killing compared with those cells without KRAS mutations. Birinapant appears to synergize with immune cells to suppress the growth of KRAS mutation-carrying cells.

To visualize the compound-induced immune cell-dependent inhibition of cancer cell growth over time, time-lapse videos of SW48-G12V cell growth were recorded in the presence of birinapant. Phase-contrast images revealed that cancer cells exhibit regular polygonal epithelial-like shape with comparable proliferation rates among control groups with PBMCs or birinapant alone, or under untreated cell culture conditions (Figures 2K and 2L; Video S1). In contrast, cancer cells underwent morphological changes, with rounding, shrinkage, and loss of adherent phenotype, upon attack by immune cells in the presence of birinapant within the initial 30 hr, and thereafter no significant cell proliferation was observed (Figures 2K and 2L; Video S1). These results demonstrate the effects of IAP-inhibitor-induced immune cell-dependent killing of cancer cells, and support the potential action of birinapant on immune cells to enhance their anti-cancer activity.

T and Natural Killer Cells Are Involved in the Birinapant-Induced Immune-Dependent Killing Effect

To determine the potential mechanism underlying the immunomodulatory effect of IAP inhibitors, we began to deconvolute the effective immune cell subtypes that might be involved in the birinapant-induced immune-dependent inhibition of cancer cell growth. Since interleukin-2 (IL-2) and anti-CD3 antibody were used in the HTiP assay as generic immune activators (Tsoukas et al., 1985), we first tested the immune selective killing effect induced by birinapant in the absence of these activators. Under the condition in which immune cells were left unstimulated, birinapant exhibited significantly reduced effect in inducing immune-dependent killing of cancer cells compared with the condition with IL-2 and anti-CD3 stimulation (Figure 3A). Given the well-documented role of IL-2 and anti-CD3 in activating T cells and natural killer (NK) cells (Bryceson et al., 2006; Smith-Garvin et al., 2009) and the potential role of IAPs in modulating T and NK

Figure 2. Identification of IAP Inhibitors as Potential Small-Molecule Immunomodulators

(A) Selectivity of 2,036 compounds in immune cell-dependent killing of SW48-G12V cells.

(B) Venn diagram of top-ranked compounds identified from image-based cell proliferation (in black) and biochemical-based cell viability (in red) readouts.

(C) Chemical structure of three small-molecule IAP inhibitors.

(D–F) Dose-dependent curves of (D) birinapant, (E) BV-6, and (F) GDC0152 for inhibiting SW48-G12V cell growth with or without PBMCs.

(G) AUC analysis of six IAP inhibitors' dose-dependent growth and viability inhibition curves.

(H and I) PBMC dose-dependent killing curves for KRAS WT and G12V isogenic SW48 cell lines with or without birinapant (1 nM) from (H) image-based cell proliferation and (I) biochemical-based cell viability readouts.

The data in D–I are presented as mean ± SEM from four independent experiments. *$p < 0.05$.

(J) AUC analysis of birinapant-induced PBMC-dependent killing curves of six patient-derived colorectal cancer cell lines from cell viability readout. WT: Caco-2, LIM1215, and SW48. G12V: SW403, SW480, and SW620. Each dot represents one cell line and the data are presented as mean ± SD. *$p < 0.05$.

(K and L) (K) Time-dependent SW48-G12V cell proliferation curves and (L) time-lapse images of SW48-G12V cell growth under the conditions as indicated. The data are presented as mean ± SEM from four replicates from a representative experiment. See also Figures S1–S3.

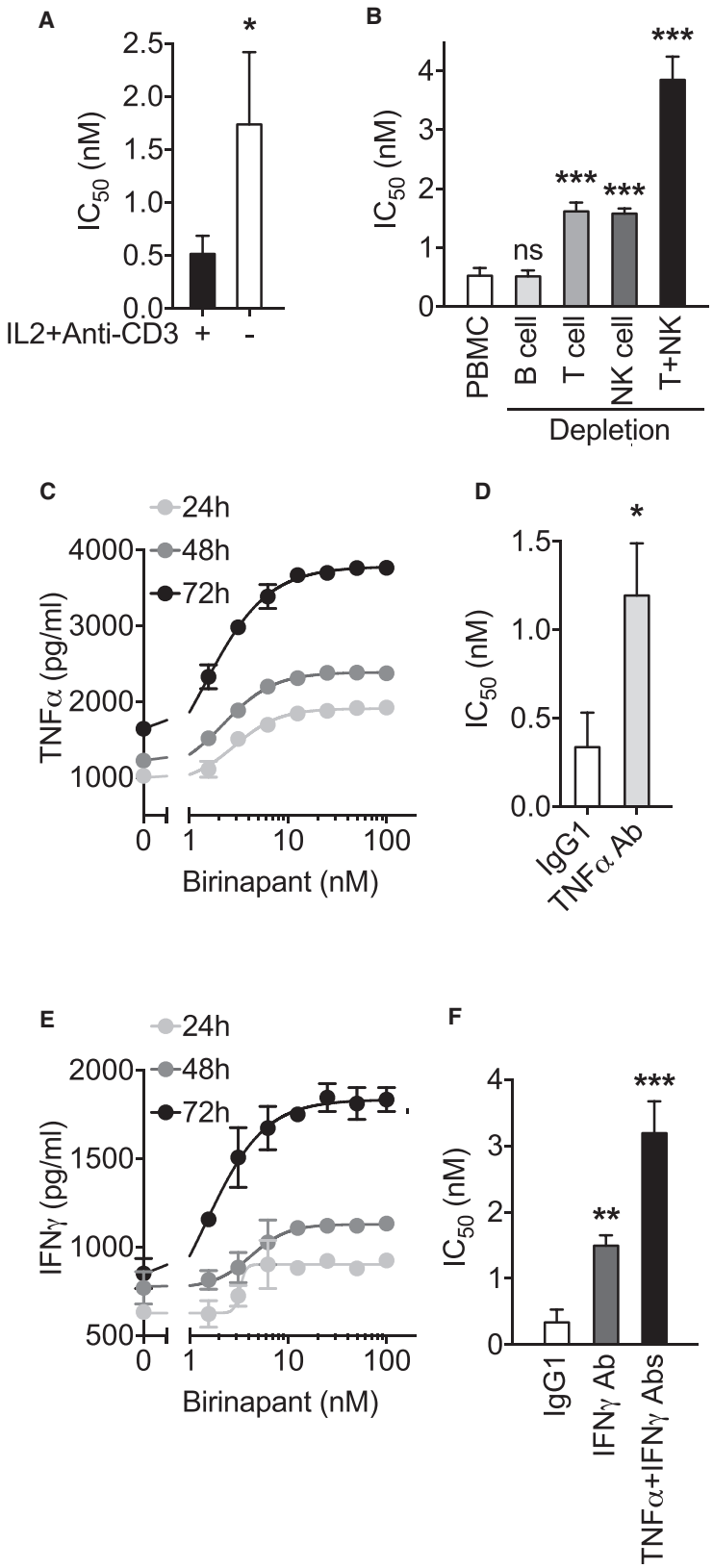

Figure 3. Identification of Effective Immune Subtypes and Cytokines Involved in Birinapant-Induced Anti-tumor Immunity

(A and B) Bar graphs showing the IC_{50} values calculated from birinapant dose-response inhibition curve (A) with (+) or without (−) immune activation using IL-2 and anti-CD3 antibody and (B) with PBMCs or depletion of immune subtypes as indicated.

(C) Dose- and time-dependent curves of TNF-α production upon birinapant stimulation.

(D) Bar graph showing the IC_{50} values calculated from birinapant dose-response inhibition curves with TNF-α neutralization using anti-TNF-α antibody.

(E) Dose- and time-dependent curves of IFN-γ production upon birinapant stimulation.

(F) Bar graph showing the IC_{50} values calculated from birinapant dose-response inhibition curves under conditions as indicated.

The data are presented as mean ± SD from three independent experiments. *$p < 0.05$, **$p < 0.01$, ***$p < 0.001$; ns, not significant.

cell activity (Dougan et al., 2010; Fischer et al., 2017), it is possible that T and NK cells might contribute to the IAP inhibitor-mediated anti-tumor immunity. Thus, we next examined the requirement of immune cell subtypes from the PBMCs for mediating birinapant-induced immunomodulation. The potency of birinapant was evaluated in the HTiP co-culture assay using PBMCs with certain immune cell subtypes depleted by magnetic beads coated with the corresponding anti-CD marker antibody. The depletion of $CD3^+$ T cells and $CD56^+$ NK cells, but not $CD19^+$ B cells, significantly increased the IC_{50} of birinapant compared with the control with intact PBMCs (Figure 3B). These results demonstrate that T and NK cells are required for the birinapant-induced effect in the immune-cancer cell interaction system.

TNF-α and IFN-γ Contribute to the Birinapant-Induced PBMC-Dependent Killing Effect

Various IAP antagonists (SMAC mimetics) have been shown to produce a synergistic effect with tumor necrosis factor alpha (TNF-α) in inducing cancer cell death (Petersen et al., 2007; Vince et al., 2007). Since we have demonstrated that the birinapant-induced immunomodulatory effects are partially mediated through the T and NK cells, and given that these cells are able to secret TNF-α (Dinarello, 2007), we next tested whether TNF-α is one of the effective cytokines in this scenario. First, we measured the TNF-α secretion from the immune and cancer cell co-culture system. Upon birinapant treatment, we observed a dose- and time-dependent increase in TNF-α concentration in the conditioned medium from the co-cultures (Figure 3C). In addition, depletion of TNF-α using 50 ng/mL TNF-α neutralizing antibody significantly attenuated the birinapant-induced PBMC-dependent inhibition of cancer cell growth (Figure 3D). These results suggested that birinapant-induced TNF-α secretion contributes to the observed immune-dependent killing of cancer cells.

In addition to TNF-α, another important immune cytokine that can be produced from T and NK cells is type II interferon (IFN-γ) (Dinarello, 2007), which has also been demonstrated to cooperate with IAP antagonists in activating cell necroptosis (Cekay et al., 2017; Tanzer et al., 2017). Similarly, we first detected a dose- and time-dependent increase in IFN-γ secretion from the co-cultures (Figure 3E). In support of this notion, inhibition of the IFN-γ signaling pathway by using IFN-γ neutralizing antibody (5 μg/mL) significantly decreased the birinapant-induced immune cell killing effect (Figure 3F). These results suggest the importance of IFN-γ in the birinapant-induced anti-tumor immune response. In addition, depletion of both TNF-α and IFN-γ together further attenuated the immunomodulatory effect of birinapant (Figure 3F). Collectively, our results suggest that TNF-α and IFN-γ are two of the effective cytokines that are important in mediating immune-dependent cancer cell death induced by an IAP antagonist.

DISCUSSION

The vast chemical space has been extensively explored to discover inhibitors of cancer cells using a variety of molecular, cellular, or phenotypic assays with tumor populations alone. It has been challenging to screen large chemical libraries using clinically relevant tumor models, particularly those with the complexity of cancer and immune system interactions. Our *in vitro* cancer and immune cell co-culture system provides a simple and scalable platform that enables its application for systematic profiling of large chemical libraries using immune cell-dependent inhibition of cancer cell growth as a phenotypic readout. The use of non-labeled native cancer and immune cells with the imaging system avoids artificial tagging-associated artifacts. The design of a built-in orthogonal detection step with the biochemical-based measurement from the same well is expected to enhance the screening efficiency and quality for hit prioritization. Promising results from the current HTiP platform that utilizes PBMCs as a source of immune cells support further development that will incorporate defined subtypes and engineered tumor antigen-specific T cells for directed screening campaigns.

Using the HTiP platform, we tested 2,036 bioactive compounds and identified three IAP antagonists as potential immunomodulators that selectively enhance the immune cell-dependent inhibition of KRAS-mutation cells. Our screening strongly supports that our co-culture HTiP platform can be applied to identify novel small-molecule immunomodulators. These IAP antagonists could serve as the first-in-class immunomodulators identified from the high-throughput screening setting and as benchmark compounds for future small-molecule immunomodulator campaigns. Meanwhile, the streamlined assay platform could be rapidly adapted and extended to a broad range of epithelial cancer cells with a wide variety of specific immune cell subtypes, such as "exhausted" T cells, $CD8^+$ cytotoxic T lymphocytes, or NK cells, or other cytotoxic organisms, such as bacteria or viruses.

In addition to IAP antagonists, it is possible that other hits might be identified if we relaxed the selection criteria. Indeed, ten different primary hits were revealed with selectivity index >1.5 but with an inhibitory effect >20% on cancer cells alone. Among these potential hits, one compound, batimastat, a matrix metalloproteinase inhibitor (Botos et al., 1996), showed immune selectivity in the dose-response study (Figure S2). This compound requires further examination with additional orthogonal assays for validation.

Because the chemical library employed contains compounds with known activities, it may offer opportunities to evaluate the performance of the screening, i.e., to assess the capture rate of known immunomodulatory compounds. However, it is challenging to define compounds with *tumor-directed* immunostimulatory activities among those known compounds at this stage due to limited knowledge in this area. Our efforts through chemoinformatics analysis did reveal (1) a known immunostimulant and (2) compounds that target proteins that are involved in immunomodulation. Pidotimod is a synthetic dipeptide with immunomodulatory properties and a demonstrated role in both innate and adaptive immunity (Ferrario et al., 2015). However, pidotimod showed <20% cancer cell killing effect in our primary screening. It needs additional experimental studies to understand whether pidotimod has tumor-directed immunogenic cell death activity. To expand the definition of the expected hits, we included compounds that are primarily not classified as immunomodulators, but act on protein targets implicated in regulating the immune response. The IAP family of proteins belongs to this class, with recently demonstrated roles in regulating

both innate and adaptive immunity, in addition to its established apoptosis inhibition function (Dougan and Dougan, 2018). In this case, IAP inhibitors could be the expected hits and indeed were identified from the HTiP platform. Other protein targets, such as phosphatidylinositol 3-kinase (PI3K) and mammalian target of rapamycin (mTOR), have been implicated in regulating immune cell fate (Koyasu, 2003; Powell et al., 2012); their corresponding compounds were not identified as hits. It should be noted that PI3K and mTOR have a broad range of biological activities, from the regulation of cell survival to protein translation. Thus, it is possible that the HTiP platform may allow the identification of compounds that target pathways selective for specific oncogenic lesions.

IAP antagonists, also known as SMAC mimetics, have been extensively studied as potential anti-cancer therapeutics in the last decade (Cheung et al., 2009; Lu et al., 2008; Petersen et al., 2007; Vince et al., 2007). However, the dramatic differences in their activities between *in vitro* 2D cell culture systems and *in vivo* human and murine cancer models when used as a single agent remain puzzling (Cheung et al., 2010; Dineen et al., 2010; Krepler et al., 2013; Lecis et al., 2013; Probst et al., 2010). The use of IAP antagonists has indicated the importance of IAP in modulating the TNF-α/nuclear factor κB-mediated inflammatory responses (Vince et al., 2007). Moreover, the significant synergistic effects between IAP inhibitors and inflammatory cytokines, such as TNF-α, IL-1β, or IFN-γ, in inhibiting cancer cell growth have implicated a potential combination strategy of using these compounds and immune stimuli to promote tumor death (Cekay et al., 2017; Cheung et al., 2010; Dineen et al., 2010; Dougan et al., 2010; Krepler et al., 2013; Lecis et al., 2013; Probst et al., 2010; Vince et al., 2007). In addition, several IAP inhibitors have recently been shown to target the immune system to evoke anti-tumor immunity in various cancer types (Beug et al., 2017; Chesi et al., 2016; Dougan et al., 2010). Our unbiased screening independently revealed three structurally distinct IAP inhibitors as potent inducers of anti-tumor immunity from our *in vitro* co-culture system, in support of the reported role of IAPs in suppression of anti-tumor immune response pathways (Dougan et al., 2010; Estornes and Bertrand, 2015; Sharma et al., 2017). The unraveling of three IAP antagonists/SMAC mimetics from our HTiP screening illustrates the power of the HTiP platform in recapitulating the complex *in vivo* immune-cancer microenvironment for the discovery of small-molecule anti-tumor immunity enhancers. The immune cell dependency of the cancer cell killing effect of these IAP antagonists strongly supports their action on the immune cell population to reverse the immune resistance of cancer cells.

SIGNIFICANCE

We have developed an HTiP platform that employs an *in vitro* immune and cancer cell co-culture system using an image-based phenotypic readout and a built-in orthogonal viability readout to monitor cancer cell growth status for accelerated discovery of small-molecule immunomodulators. The identification of multiple IAP antagonists/SMAC mimetics, with demonstrated roles as anti-tumor immunity enhancers, supports the validity of the HTiP system for the accelerated discovery of small-molecule anti-cancer immune-enhancing compounds. This platform could be readily adapted to a wide range of immune and cancer cell types with various genetic backgrounds for the identification of small-molecule immunomodulators or studying immune surveillance mechanisms toward personalized immunotherapy.

STAR★METHODS

Detailed methods are provided in the online version of this paper and include the following:

- KEY RESOURCES TABLE
- CONTACT FOR REAGENT AND RESOURCE SHARING
- EXPERIMENTAL MODEL AND SUBJECT DETAILS
- METHOD DETAILS
  - Immune and Tumor Cell Co-culture Assay
  - Cell Proliferation Measurement
  - Cell Viability Measurement
  - The Emory Enriched Bioactive Library and Other Chemicals
  - HTiP Method for Small Molecule Immunomodulator Discovery
  - Time-Lapse Video for Cell Proliferation Kinetics
  - Immune Cell Subtype and Cytokine Depletion Assays
- QUATIFICATION AND STATISTICAL ANALYSIS

SUPPLEMENTAL INFORMATION

Supplemental Information includes three figures and one video and can be found with this article online at https://doi.org/10.1016/j.chembiol.2018.11.011.

ACKNOWLEDGMENTS

We would like to thank Dr. Andrey A. Ivanov (Department of Pharmacology and Emory Chemical Biology Discovery Center) for chemoinformatic analysis of EEBL. This research was supported in part by NIH NCI U01CA217875, NIH NCI 5U01CA199241 and a Georgia Cancer Coalition Award from Georgia Research Alliance, the Emory Chemical Biology Discovery Center, and Winship Cancer Institute of Emory University (NIH 5P30CA138292).

AUTHOR CONTRIBUTIONS

Conceptualization, X.M. and H.F.; Methodology, X.M., Y.D., and H.F.; Investigation, X.M., C.T., Q.N., T.M., and Y.D.; Writing - original draft, X.M. and H.F.; Writing - review & editing, X.M., C.T., Q.N., T.M., Y.D., and H.F.; Funding acquisition, H.F.; Resources, H.F.; Supervision, X.M. and H.F.

DECLARATION OF INTERESTS

The authors declare no competing interests.

Received: May 10, 2018
Revised: October 8, 2018
Accepted: November 16, 2018
Published: January 10, 2019

REFERENCES

Beug, S.T., Beauregard, C.E., Healy, C., Sanda, T., St-Jean, M., Chabot, J., Walker, D.E., Mohan, A., Earl, N., Lun, X., et al. (2017). Smac mimetics synergize with immune checkpoint inhibitors to promote tumour immunity against glioblastoma. Nat. Commun. *8*, https://doi.org/10.1038/ncomms14278.

Botos, I., Scapozza, L., Zhang, D., Liotta, L.A., and Meyer, E.F. (1996). Batimastat, a potent matrix metalloproteinase inhibitor, exhibits an unexpected mode of binding. Proc. Natl. Acad. Sci. U S A *93*, 2749–2754.

Bryceson, Y.T., March, M.E., Ljunggren, H.G., and Long, E.O. (2006). Activation, coactivation, and costimulation of resting human natural killer cells. Immunol. Rev. *214*, 73–91.

Cekay, M.J., Roesler, S., Frank, T., Knuth, A.K., Eckhardt, I., and Fulda, S. (2017). Smac mimetics and type II interferon synergistically induce necroptosis in various cancer cell lines. Cancer Lett. *410*, 228–237.

Chames, P., Van Regenmortel, M., Weiss, E., and Baty, D. (2009). Therapeutic antibodies: successes, limitations and hopes for the future. Br. J. Pharmacol. *157*, 220–233.

Chen, N., Fang, W., Lin, Z., Peng, P., Wang, J., Zhan, J., Hong, S., Huang, J., Liu, L., Sheng, J., et al. (2017). KRAS mutation-induced upregulation of PD-L1 mediates immune escape in human lung adenocarcinoma. Cancer Immunol. Immunother. *66*, 1175–1187.

Chesi, M., Mirza, N.N., Garbitt, V.M., Sharik, M.E., Dueck, A.C., Asmann, Y.W., Akhmetzyanova, I., Kosiorek, H.E., Calcinotto, A., Riggs, D.L., et al. (2016). IAP antagonists induce anti-tumor immunity in multiple myeloma. Nat. Med. *22*, 1411–1420.

Cheung, H.H., Beug, S.T., St Jean, M., Brewster, A., Kelly, N.L., Wang, S., and Korneluk, R.G. (2010). Smac mimetic compounds potentiate interleukin-1beta-mediated cell death. J. Biol. Chem. *285*, 40612–40623.

Cheung, H.H., Mahoney, D.J., Lacasse, E.C., and Korneluk, R.G. (2009). Down-regulation of c-FLIP enhances death of cancer cells by Smac mimetic compound. Cancer Res. *69*, 7729–7738.

Dhanak, D., Edwards, J.P., Nguyen, A., and Tummino, P.J. (2017). Small-molecule targets in immuno-oncology. Cell Chem. Biol. *24*, 1148–1160.

Dinarello, C.A. (2007). Historical insights into cytokines. Eur. J. Immunol. *37* (*Suppl 1*), S34–S45.

Dineen, S.P., Roland, C.L., Greer, R., Carbon, J.G., Toombs, J.E., Gupta, P., Bardeesy, N., Sun, H., Williams, N., Minna, J.D., et al. (2010). Smac mimetic increases chemotherapy response and improves survival in mice with pancreatic cancer. Cancer Res. *70*, 2852–2861.

Dougan, M., Dougan, S., Slisz, J., Firestone, B., Vanneman, M., Draganov, D., Goyal, G., Li, W., Neuberg, D., Blumberg, R., et al. (2010). IAP inhibitors enhance co-stimulation to promote tumor immunity. J. Exp. Med. *207*, 2195–2206.

Dougan, S.K., and Dougan, M. (2018). Regulation of innate and adaptive anti-tumor immunity by IAP antagonists. Immunotherapy *10*, 787–796.

Estornes, Y., and Bertrand, M. (2015). IAPs, regulators of innate immunity and inflammation. Semin. Cell Dev. Biol. *39*, 106–114.

Ferrario, B.E., Garuti, S., Braido, F., and Canonica, G.W. (2015). Pidotimod: the state of art. Clin. Mol. Allergy *13*, 8.

Fesnak, A.D., June, C.H., and Levine, B.L. (2016). Engineered T cells: the promise and challenges of cancer immunotherapy. Nat. Rev. Cancer *16*, 566–581.

Fischer, K., Tognarelli, S., Roesler, S., Boedicker, C., Schubert, R., Steinle, A., Klingebiel, T., Bader, P., Fulda, S., and Ullrich, E. (2017). The Smac mimetic BV6 improves NK cell-mediated killing of rhabdomyosarcoma cells by simultaneously targeting tumor and effector cells. Front. Immunol. *8*, 202.

Huxley, P., Sutton, D.H., Debnam, P., Matthews, I.R., Brewer, J.E., Rose, J., Trickett, M., Williams, D.D., Andersen, T.B., and Classon, B.J. (2004). High-affinity small molecule inhibitors of T cell costimulation: compounds for immunotherapy. Chem. Biol. *11*, 1651–1658.

Kortlever, R.M., Sodir, N.M., Wilson, C.H., Burkhart, D.L., Pellegrinet, L., Brown Swigart, L., Littlewood, T.D., and Evan, G.I. (2017). Myc cooperates with Ras by programming inflammation and immune suppression. Cell *171*, 1301–1315.e14.

Koyasu, S. (2003). The role of PI3K in immune cells. Nat. Immunol. *4*, 313–319.

Krepler, C., Chunduru, S.K., Halloran, M.B., He, X., Xiao, M., Vultur, A., Villanueva, J., Mitsuuchi, Y., Neiman, E.M., Benetatos, C., et al. (2013). The novel SMAC mimetic birinapant exhibits potent activity against human melanoma cells. Clin. Cancer Res. *19*, 1784–1794.

Lecis, D., De Cesare, M., Perego, P., Conti, A., Corna, E., Drago, C., Seneci, P., Walczak, H., Colombo, M.P., Delia, D., et al. (2013). Smac mimetics induce inflammation and necrotic tumour cell death by modulating macrophage activity. Cell Death Dis. *4*, e920.

Lu, J., Bai, L., Sun, H., Nikolovska-Coleska, Z., McEachern, D., Qiu, S., Miller, R.S., Yi, H., Shangary, S., Sun, Y., et al. (2008). SM-164: a novel, bivalent Smac mimetic that induces apoptosis and tumor regression by concurrent removal of the blockade of cIAP-1/2 and XIAP. Cancer Res. *68*, 9384–9393.

Nikolovska-Coleska, Z., Xu, L., Hu, Z., Tomita, Y., Li, P., Roller, P.P., Wang, R., Fang, X., Guo, R., Zhang, M., et al. (2004). Discovery of embelin as a cell-permeable, small-molecular weight inhibitor of XIAP through structure-based computational screening of a traditional herbal medicine three-dimensional structure database. J. Med. Chem. *47*, 2430–2440.

Petersen, S.L., Wang, L., Yalcin-Chin, A., Li, L., Peyton, M., Minna, J., Harran, P., and Wang, X. (2007). Autocrine TNFalpha signaling renders human cancer cells susceptible to Smac-mimetic-induced apoptosis. Cancer Cell *12*, 445–456.

Postow, M., Callahan, M., and Wolchok, J. (2015). Immune checkpoint blockade in cancer therapy. J. Clin. Oncol. *33*, 1974–1982.

Powell, J.D., Pollizzi, K.N., Heikamp, E.B., and Horton, M.R. (2012). Regulation of immune responses by mTOR. Annu. Rev. Immunol. *30*, 39–68.

Probst, B.L., Liu, L., Ramesh, V., Li, L., Sun, H., Minna, J.D., and Wang, L. (2010). Smac mimetics increase cancer cell response to chemotherapeutics in a TNF-alpha-dependent manner. Cell Death Differ. *17*, 1645–1654.

Sadelain, M., Riviere, I., and Riddell, S. (2017). Therapeutic T cell engineering. Nature *545*, 423–431.

Sharma, S., Kaufmann, T., and Biswas, S. (2017). Impact of inhibitor of apoptosis proteins on immune modulation and inflammation. Immunol. Cell Biol. *95*, 236–243.

Skalniak, L., Zak, K.M., Guzik, K., Magiera, K., Musielak, B., Pachota, M., Szelazek, B., Kocik, J., Grudnik, P., Tomala, M., et al. (2017). Small-molecule inhibitors of PD-1/PD-L1 immune checkpoint alleviate the PD-L1-induced exhaustion of T-cells. Oncotarget *8*, 72167–72181.

Smith-Garvin, J.E., Koretzky, G.A., and Jordan, M.S. (2009). T cell activation. Annu. Rev. Immunol. *27*, 591–619.

Tanzer, M.C., Khan, N., Rickard, J.A., Etemadi, N., Lalaoui, N., Spall, S.K., Hildebrand, J.M., Segal, D., Miasari, M., Chau, D., et al. (2017). Combination of IAP antagonist and IFNgamma activates novel caspase-10- and RIPK1-dependent cell death pathways. Cell Death Differ. *24*, 481–491.

Tsoukas, C.D., Landgraf, B., Bentin, J., Valentine, M., Lotz, M., Vaughan, J.H., and Carson, D.A. (1985). Activation of resting T lymphocytes by anti-CD3 (T3) antibodies in the absence of monocytes. J. Immunol. *135*, 1719–1723.

Vince, J.E., Wong, W.W., Khan, N., Feltham, R., Chau, D., Ahmed, A.U., Benetatos, C.A., Chunduru, S.K., Condon, S.M., McKinlay, M., et al. (2007). IAP antagonists target cIAP1 to induce TNFalpha-dependent apoptosis. Cell *131*, 682–693.

Zdanov, S., Mandapathil, M., Abu Eid, R., Adamson-Fadeyi, S., Wilson, W., Qian, J., Carnie, A., Tarasova, N., Mkrtichyan, M., Berzofsky, J.A., et al. (2016). Mutant KRAS conversion of conventional T cells into regulatory T cells. Cancer Immunol. Res. *4*, 354–365.

Zhang, J.H., Chung, T.D., and Oldenburg, K.R. (1999). A simple statistical parameter for use in evaluation and validation of high throughput screening assays. J. Biomol. Screen. *4*, 67–73.

STAR★METHODS

KEY RESOURCES TABLE

REAGENT or RESOURCE	SOURCE	IDENTIFIER
Antibodies		
Mouse monoclonal anti-β-Actin antibody	Sigma-Aldrich	Cat# A2228; RRID: AB_476697
Rabbit polyclonal anti-KRAS antibody	Proteintech	Cat# 12063-1-AP; RRID: AB_878040
Rabbit monoclonal anti-KRAS (G12V specific) antibody	Cell signaling	Cat# 14412S; RRID: AB_2714031
Human TNFα neutralization mouse monoclonal antibody	R&D Systems	Cat# MAB201-100
Human IFNγ neutralization mouse monoclonal antibody	Thermo Fisher	Cat# 14-7318-81; RRID: AB_468475
Mouse IgG1 isotype control	Thermo Fisher	Cat# 02-6100; RRID: AB_2532935
CD3 monoclonal antibody (OKT3)	Thermo Fisher	Cat# 16-0037-81; RRID: AB_468854
Chemicals, Peptides, and Recombinant Proteins		
Human recombinant IL-2	PeproTech	Cat# 200-02
Birinapant	Selleckchem	Cat# S7015
BV-6	Selleckchem	Cat# S7597
GDC0152	Selleckchem	Cat# S7010
AZD5582	Selleckchem	Cat# S7362
LCL161	Selleckchem	Cat# S7009
AT406	Selleckchem	Cat# S2754
EEBL	Emory ECBDC	N/A
Batimastat	Selleckchem	Cat# S7155
Critical Commercial Assays		
CellTiter-Blue® Cell Viability Assay	Promega	Cat# G8081
TNFα Human ELISA Kit	Thermo Fisher	Cat# KHC3011
IFNγ Human ELISA Kit	Thermo Fisher	Cat# EHIFNG
Experimental Models: Cell Lines		
Human KRAS (G12V/+) SW48 Cell Lines	Horizon Discovery	Cat# HD 103-007
Human KRAS (G12V/+) LIM1215 Cell Lines	Horizon Discovery	Cat# HD 116-006
Human KRAS (G12V/+9n) NCI-H838 Cell Line	Horizon Discovery	Cat# HD 114-003
Caco-2	ATCC	Cat# HTB-37
SW403	ATCC	Cat# CCL-230
SW480	ATCC	Cat# CCL-228
SW620	ATCC	Cat# CCL-227
Peripheral Blood Mononuclear Cells, Human, Normal	ATCC	Cat# PCS-800-011
Software and Algorithms		
Graphpad Prism	Graphpad; v7	https://www.graphpad.com/scientific-software/prism/
IncuCyte S3 software	Essen BioScience; S3	https://www.essenbioscience.com/en/products/software/incucyte-s3-software-v2018b/
Final Cut Pro X	Apple	https://www.apple.com/final-cut-pro/
Other		
Dynabeads™ CD3	Thermo Fisher	Cat# 11151D
MagniSort™ Human CD56 Positive Selection Kit	Thermo Fisher	Cat# 8802-6835-74
Dynabeads™ CD19 Pan B	Thermo Fisher	Cat# 11143D

CONTACT FOR REAGENT AND RESOURCE SHARING

Further information and requests for resources and reagents should be directed to and will be fulfilled by the Lead Contact, Haian Fu (hfu@emory.edu).

EXPERIMENTAL MODEL AND SUBJECT DETAILS

All cells were grown at 37°C and 5% CO_2. The X-MAN® KRAS isogenic cell lines, including two human colorectal adenocarcinoma cells SW48 (female) and LIM1215 (male) and one human lung adenocarcinoma cell NCI-H838 (male) and their corresponding genomic engineered counterparts with the heterozygous knockin of KRAS G12V activating mutation, were from Horizon Discovery (Cambridge, UK) and maintained according to manufacturer's protocol. Four additional patient-derived human colorectal adenocarcinoma cell lines, including Caco-2 (male), SW403 (female), SW480 (male) and SW620 (male), were purchased from the American Type Culture Collection (ATCC). The authenticity of these cell lines was verified by western blot using KRAS-G12V specific antibody (Cell Signaling #14412S) (Figure S3). The primary Peripheral Blood Mononuclear Cells (PBMC) from healthy donor (ATCC PCS-800-011™) were recovered from liquid nitrogen and were used immediately for co-culturing with cancer cells in T cell medium, which is Roswell Park Memorial Institute (RPMI) 1640 medium containing L-glutamine (CORNING Cat# 10-040) supplemented with 10% fetal bovine serum and 100 units/ml of penicillin/streptomycin.

METHOD DETAILS

Immune and Tumor Cell Co-culture Assay

PBMCs as effector immune cells and KRAS isogenic cancer cells as target cells were used for co-culture assays. Tumor cells were seeded at specific density in 384-well cell culture plate (Corning #3764). Twenty-four hours later, PBMCs were then thawed and co-cultured in T-cell medium with tumor cells in a dose dependent manner for four days. CD3 monoclonal antibody (100 ng/mL, OKT3, ThermoFisher) and human recombinant interleukin-2 (10 ng/mL, PeproTech) were used as activation cocktail to activate immune cells.

Cell Proliferation Measurement

The co-culture assay plates were imaged using the IncuCyte® S3 Live-Cell Analysis System (Essen Biosciences). The cancer cell proliferation was monitored and characterized as the percentage of confluence using the IncuCyte® basic analysis module. Because of the size distinction between effector immune cells and target cancer cells, the area filter of >400 μm^2 was used to select cancer cells that are larger in size.

Cell Viability Measurement

Cell Titer Blue (Promega, G8081) was added to each well. The plates were incubated for desired time at 37°C to allow the generation of sufficient signal within the linear range. The fluorescence intensity of each well was read using an PHERAstar *FSX* multi-mode plate reader (Ex 545 nm, Em 615 nm; BMG LABTECH). Cells containing medium or immune cells alone were used as blank control for background correction.

The Emory Enriched Bioactive Library and Other Chemicals

The Emory Enriched Bioactive Library (EEBL) consists of a collection of 2036 diverse small molecules with validated biological and pharmacological activities, including 1018 FDA approved compounds (Selleckchem). These molecules are focused on over two hundred targets that are part of more than twenty signaling pathways, including survival and apoptosis pathways. The selected primary hits were re-ordered from Selleckchem for validation studies. Additional IAP inhibitors, AT406, AZD5582 and LCL161, were purchased from Selleckchem.

HTiP Method for Small Molecule Immunomodulator Discovery

For the primary screening, SW48-G12V cells were seeded in 384-well cell culture plate (1,000 cells/well in 40 μl medium; Corning, Cat#3764) using a Multidrop Combi Reagent Dispenser (ThermoScientific). The last column was used as a medium or PBMCs only control (blk). The next day, PBMCs were dispensed at 5,000 cells/well in 10 μl media containing the activation cocktail. Subsequently, the 2036 Emory Enriched Bioactive Library (EEBL) compounds (100 nl) were added into wells in each plate using Biomek NXP Automated Workstation (Beckman) from a compound stock plate to give the final concentration of 2 μM. The final DMSO concentration was 0.2% (v/v) in samples with compound treatment. Each sample was tested with single point. A parallel screening was performed with SW48-G12V cells alone (1000 cells/well) in 50 μl medium containing the same amount of activation cocktail in the absence of PBMCs. After 4 days of incubation, image-based cell proliferation readouts followed by biochemical-based cell viability measurements were used to examine the compound effect on cancer cell growth. Z' factor was calculated as

$$Z' = 1 - \frac{3 \times (SD_{positive} + SD_{blank})}{S_{positive} - S_{blank}}$$

Where $SD_{positive}$ and SD_{blank} are the standard deviations, and $S_{positive}$ and S_{blank} are the corresponding average of the cell confluence or fluorescence intensity for wells with DMSO containing PBMCs/medium only or plus cancer cells, respectively. A Z' factor between 0.5 and 1.0 indicates that the assay is suitable for HTS (Zhang et al., 1999). The percentage of control (%C) was calculated using the equation $100X(S_{compound}-S_{blank})/(S_{positive}-S_{blank})$. The immune killing selectivity index was calculated using the equation $\log_{10}(\%C_{-PBMC}/\%C_{+PBMC})$.

Time-Lapse Video for Cell Proliferation Kinetics

SW48-G12V cells were plated in 96-well IncuCyte® ImageLock plates (Essen Biosciences, #4379) at 6,000 cells per wells. Twenty-four hours later, cells were treated with various conditions as indicated and imaged with time-lapse setting using the IncuCyte® S3 Live-Cell Analysis System (Essen Biosciences). PBMCs were added at 30,000 cells/well containing the activation cocktail. Birinapant with final concentration of 5 nM was used with the final DMSO concentration of 0.1% (v/v). The time-lapse video was composed by displaying images at 6 frames per second using Final Cut Pro X software.

Immune Cell Subtype and Cytokine Depletion Assays

PBMCs depleted with $CD3^+$ T cells, $CD56^+$ NK cells, or $CD19^+$ B cells were obtained by incubating the primary PBMCs with magnetic beads coated with anti-CD3, CD56 or CD19 antibody (ThermoFisher Scientific), respectively, according to the manufacturer's instruction. The human TNFα neutralization mouse monoclonal antibody was purchased from R&D Systems (#MAB210-100). The human IFNγ neutralization mouse monoclonal antibody and mouse IgG1 isotype control were purchased from ThermoFisher. For Enzyme-linked immunosorbent assay (ELISA) assay, the conditioned medium from the co-culture assay upon the treatment with compound or controls was collected and centrifuged to remove any cells or debris. Then the supernatant was analyzed for the TNFα and IFNγ amount using the TNF alpha and IFN gamma Human ELISA Kit (ThermoFisher Scientific), respectively, according to manufacturer's protocol.

QUATIFICATION AND STATISTICAL ANALYSIS

The dose-dependent PBMC-induced or small molecule induced cancer cell growth inhibition curve was established using GraphPad Prism based on the Sigmoidal dose-response (variable slope) equation. For quantitative analysis of the dose response, the area under the curve (AUC) was computed as a measurement of cancer growth signal, as AUC integrates both the amplitude and shape of the growth curve. The student's t-test was used for statistics and P-value of 0.05 or less were considered statistically significant.

Cell Chemical Biology, Volume *26*

Supplemental Information

HTiP: High-Throughput Immunomodulator Phenotypic Screening Platform to Reveal IAP Antagonists as Anti-cancer Immune Enhancers

Xiulei Mo, Cong Tang, Qiankun Niu, Tingxuan Ma, Yuhong Du, and Haian Fu

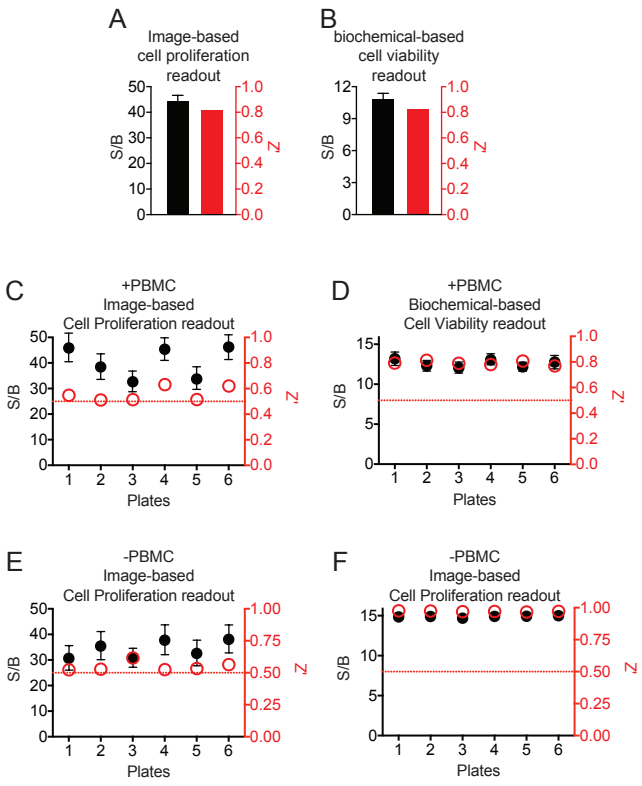
A
Image-based
cell proliferation
readout
S/B
Z
B
biochemical-based
cell viability
readout
S/B
Z
C
+PBMC
Image-based
Cell Proliferation readout
S/B
Z'
Plates
D
+PBMC
Biochemical-based
Cell Viability readout
S/B
Z'
Plates
E
-PBMC
Image-based
Cell Proliferation readout
S/B
Z'
Plates
F
-PBMC
Image-based
Cell Proliferation readout
S/B
Z'
Plates

Figure S1. Assay and screening performance evaluation, related to Figure 1 and 2.

(A-B) S/B and Z' calculated at PBMC/cancer cell ratio of 5 from **(A)** image- and **(B)** biochemical-based readouts. The data are presented as mean ± SD from 4 replicate wells. **(C-F)** S/B and Z' calculated from six independent assay plates in the presence (**C** and **D**) or the absence (**E** and **F**) of PBMC using the image-based cell proliferation readouts (**C** and **E**) or the biochemical-based cell viability readouts (**D** and **F**). The data are presented as mean ± SD from 16 replicate wells. For dots that show no error bar, the error bar was smaller than the dot.

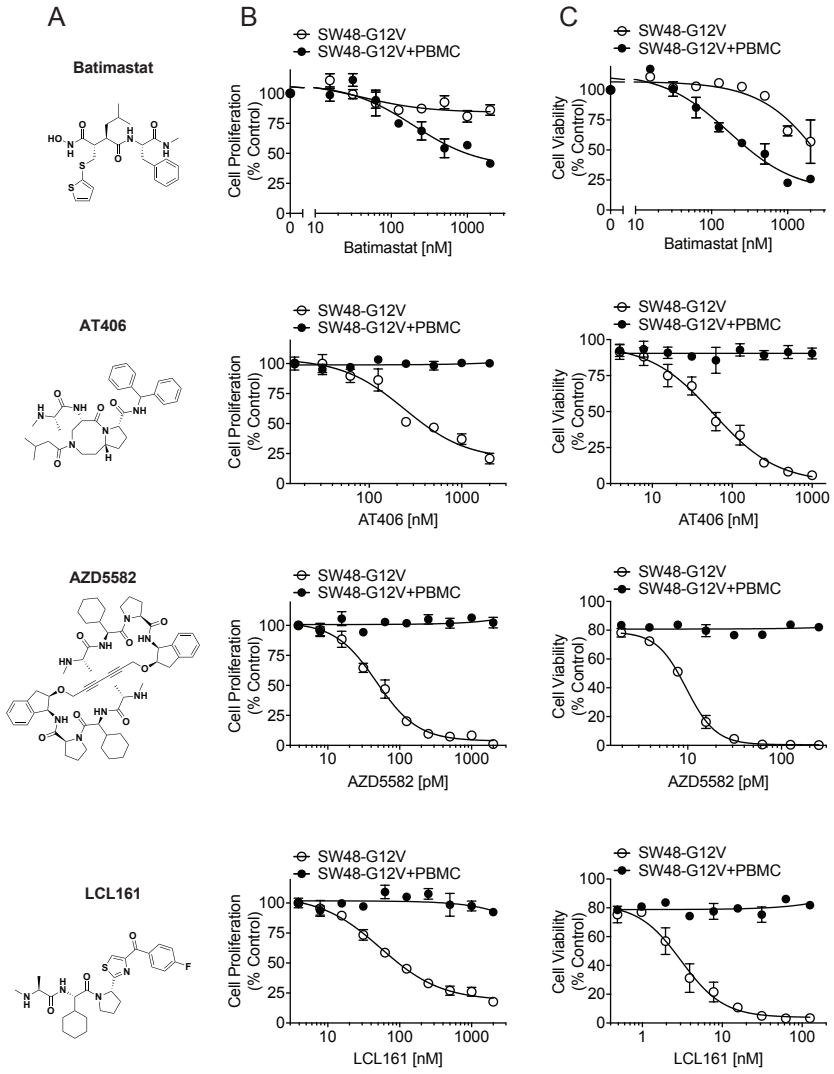
A
B
C
Batimastat
AT406
AZD5582
LCL161
SW48-G12V
SW48-G12V+PBMC
Cell Proliferation (% Control)
Cell Viability (% Control)
Batimastat [nM]
AT406 [nM]
AZD5582 [pM]
LCL161 [nM]

Figure S2. Dose-response curves of batimastat and three additional IAP antagonists in HTiP assay, related to Figure 2. (A) Chemical structure of the compounds as indicated. **(B-C)** The corresponding dose-dependent inhibition curves of SW48-G12V cell growth from **(B)** image-based cell proliferation and **(C)** biochemical-based cell viability readouts. The data are presented as mean ± SEM from four replicate wells.

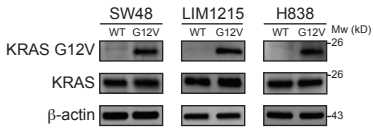
SW48
LIM1215
H838
WT G12V
WT G12V
WT G12V
Mw (kD)
KRAS G12V
KRAS
β-actin
26
26
43

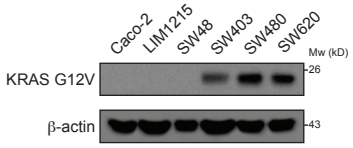
Caco-2
LIM1215
SW48
SW403
SW480
SW620
Mw (kD)
KRAS G12V
β-actin
26
43

Figure S3. Cell line authentication, related to Figure 1 and 2. The authenticity of the genomic-engineered KRAS-G12V isogenic cell lines and patient-derived colorectal cancer cell lines was experimentally verified by western blotting of the cell lysates using KRAS-G12V or pan-KRAS antibody.